Available online at www.sciencedirect.com
ScienceDirect
Applied Catalysis B: Environmental 81 (2008) 141–149
APPLIED CATALYSIS B: ENVIRONMENTAL
www.elsevier.com/locate/apcatb

Catalytic reduction of NO by CO over NiO/CeO_2 catalyst in stoichiometric NO/CO and $NO/CO/O_2$ reaction

Yong Wang [a], Aimin Zhu [a], Yuzhuo Zhang [a], C.T. Au [b], Xuefeng Yang [a], Chuan Shi [a,*]

[a] *Laboratory of Plasma Physical Chemistry, Dalian University of Technology, Dalian 116024, China*
[b] *Department of Chemistry, Center for Surface Analysis and Research Hong Kong, Baptist University, Kowloon Tong, Hong Kong*

Received 18 May 2007; received in revised form 15 November 2007; accepted 1 December 2007
Available online 23 December 2007

Abstract

A new catalyst composed of nickel oxide and cerium oxide was studied with respect to its activity for NO reduction by CO under stoichiometric conditions in the absence as well as the presence of oxygen. Activity measurements of the NO/CO reaction were also conducted over $NiO/\gamma\text{-}Al_2O_3$, NiO/TiO_2, and NiO/CeO_2 catalysts for comparison purposes. The results showed that the conversion of NO and CO are dependent on the nature of supports, and the catalysts decreased in activity in the order of $NiO/CeO_2 > NiO/\gamma\text{-}Al_2O_3 > NiO/TiO_2$. Three kinds of CeO_2 were prepared and used as support for NiO. They are the CeO_2 prepared by (i) homogeneous precipitation (HP), (ii) precipitation (PC), and (iii) direct decomposition (DP) method. We found that the NiO/CeO_2(HP) catalyst was the most active, and complete conversion of NO and CO occurred at 210 °C at a space velocity of 120,000 h^{-1}. Based on the results of surface analysis, a reaction model for NO/CO interaction over NiO/CeO_2 has been proposed: (i) CO reduces surface oxygen to create vacant sites; (ii) on the vacant sites, NO dissociates to produce N_2; and (iii) the oxygen originated from NO dissociation is removed by CO.
© 2008 Published by Elsevier B.V.

Keywords: NO reduction; CO; NiO/CeO_2 catalyst

1. Introduction

With the use of three-way catalysts (TWCs), the release of nitrogen oxides has been significantly reduced. Precious metals Pt, Pd, and Rh supported on alumina and ceria [1–5] have long been considered as the most efficient for the control of exhaust gas. For such application, ceria-related compounds are believed to operate mainly as redox facilitators [6–9] or structural promoters of the active metals (or metal oxides) with which they are in contact [10,11]. The promotion effect of ceria is related to the particular redox properties acquired by the system upon establishment of metal–ceria contacts [12,13]. There are reports on ceria participation in water–gas shift [14,15], CO oxidation [16,17], as well as NO reduction [18–21] reactions. Due to the high cost of precious metals, considerable efforts have been paid to the utilization of ceria-supported transition metals and their oxides, and cases of ceria-supported V [22–23], Cu [24–27], Ag [28,29], Cr [30–32], Co [33] have been reported.

Generally speaking, there are two kinds of mechanistic models for the reduction of NO by CO over TWCs [34]. One involves NO dissociative adsorption [35–38] and the other catalyst-assisted decomposition of molecularly adsorbed NO in the presence of a reductant [39,40]. Over Rh/CeO_2 [41], for example, nitric oxide can either adsorb dissociatively on metallic sites, leading to the generation of oxygen and nitrogen adatoms, or adsorb associatively on cationic sites, leading to the formation of dinitrosyl or hyponitrite species. On cationic sites, successive cleavage of N–O bonds of dinitrosyl or hyponitrite species occurs, plausibly leading to the generation of N_2O; in all cases the oxygen atoms left on the active sites inhibit further adsorption of NO. A reductant is then required to remove the oxygen atoms for the reaction to proceed further. On metallic sites, NO undergoes dissociative chemisorption, leading to surface nitrogen and oxygen atoms. Again, a reductant is necessary to remove the oxygen.

* Corresponding author. Tel.: +86 411 84708548; fax: +86 411 84708548/808.
E-mail address: chuanshi@dlut.edu.cn (C. Shi).

0926-3373/$ – see front matter © 2008 Published by Elsevier B.V.
doi:10.1016/j.apcatb.2007.12.005

Among the catalysts of non-noble metals, copper in the form of oxide and as a supported active component have been a focus of investigation [42,43]. On catalysts of base metal oxides, the reduction of NO in the presence of CO is believed to proceed in two steps, first partial reduction of NO to give N_2O, and then subsequent reduction of N_2O to produce N_2. As on catalysts of supported copper, the reaction between NO and CO involves the primary step of NO decomposition to give O and N adatoms. Subsequently, surface oxygen reacts with CO to produce CO_2, thereby making available the Cu surface sites for further reaction with NO.

With facile redox actions, catalysts of nickel oxide supported on ceria have been studied for many hydrogenation reactions [44,45] and oxidation reactions [46]. However, reports on the use of the catalysts for NO reduction by CO are rare. In this paper, we report the optimization of ceria-supported NiO for stoichiometric NO/CO and NO/CO/O_2 reactions, focusing on, in particular, the synergistic effect of NiO and ceria and the mechanism of the reaction. In this study, the catalytic activities for CO oxidation and NO reduction over NiO supported on γ-Al_2O_3, TiO_2(P25), and the CeO_2 samples prepared by different methods were examined. TPR and XRD measurements were adopted to characterize the structure properties of the catalysts, and the mechanism of the NO/CO reaction was investigated by IR and MS techniques.

2. Experimental

2.1. Materials

The supports were γ-Al_2O_3, TiO_2, and CeO_2. The γ-Al_2O_3 material was provided by Wenzhou Factory, China and was calcined at 500 °C for 3 h in air before use. The TiO_2 used was Degussa P25. The NiO sample was obtained by decomposing $Ni(NO_3)_3{\cdot}6H_2O$ in air at 500 °C in a span of 3 h. There were a total of three CeO_2 samples prepared by three different methods. The one denoted as CeO_2(DP) hereinafter was obtained by calcining $Ce(NO_3)_3{\cdot}6H_2O$ in air at 500 °C for 3 h (denoted hereinafter as DP method). The ceria denoted as CeO_2(PC) was synthesized by having CeO_2 precipitated when ammonia (26–28 wt%) was added to a 0.5 M aqueous solution of $Ce(NO_3)_3{\cdot}6H_2O$ (to reach a pH of 10) at room temperature (denoted as PC method). The precipitate was filtered out and washed with deionized water (to reach a pH of between 7 and 8), and then with ethanol before being dried at 110 °C overnight and calcined at 500 °C in air for 3 h. The ceria sample denoted as CeO_2(HP) was prepared by homogenous precipitation (denoted as HP method): 0.3 M urea and 0.05 M $Ce(NO_3)_3{\cdot}6H_2O$ solution were added to a three-neck flask. After constant stirring for 10 h at 80 °C, there was the appearance of a white precipitate, and the temperature of the mixture was kept at 80 °C for an additional 2–3 h for aging. The solid substance was then filtered out, washed, dried and calcined according to the procedure of CeO_2(PC) generation.

The CeO_2-supported NiO catalysts were prepared via wetness impregnation using $Ni(NO_3)_3{\cdot}6H_2O$ as precursor salt. The obtained samples were dried in an oven at 120 °C for over 8 h, pressed, sieved, and finally calcined at 500 °C for 1 h in He atmosphere before being tested. The nominal Ni loading of the catalysts was ca. 7 wt%. The catalysts are denoted hereinafter as NiO/γ-Al_2O_3, NiO/TiO_2, NiO/CeO_2(DP), NiO/CeO_2(PC), and NiO/CeO_2(HP).

2.2. Techniques

The tests for catalytic activity were carried out at atmospheric pressure over a fixed-bed flow system. The catalyst (100 mg, 40–60 mesh) was placed in a quartz reactor (id: 4 mm) equipped with devices for temperature measurement and control. Typical feeds (total gas flow rate: 75 $cm^3\,min^{-1}$; i.e. space velocity: 120,000 h^{-1}) were (i) NO:CO = 0.25%:0.25% with He balance, and (ii) NO:CO:O_2 = 0.25%:0.5%:0.125% with He balance (in volume to volume ratio). Before each test, the catalyst was heated to 500 °C at a rate of 15 °C min^{-1} and was held at this temperature for 1 h in a flow of He. During the reaction, a period of 25 min was allowed for the reaction to reach stabilization after each change of temperature. The gases exited from the reactor were analyzed by GC equipped with a TCD detector. The catalytic activity was calculated according to the following formula:

$$CO_{conv.} = \frac{[CO]_{in} - [CO]_{out}}{[CO]_{in}} \times 100\%$$

$$NO_{conv.} = \frac{2[N_2]_{out}}{[NO]_{in}} \times 100\%$$

the subscript "in" denotes initial concentration whereas "out" means after reaction. To serve as an illustration, $[N_2]_{out}$ denotes the concentration of N_2 after reaction.

X-ray diffraction (XRD) data were obtained on a Rigaku D/max-rA powder diffractometer with Cu Kα radiation. The patterns were collected at 25 °C over a 2θ range of 20–80° with a step interval of 0.06°. Temperature-programmed reduction (TPR) experiments were performed on a system equipped with a TCD detector employing 3 vol.% H_2 in nitrogen at a flow rate of 50 $cm^3\,min^{-1}$. The catalyst (30 mg) was pre-treated in He stream at 500 °C for 1 h and then cooled to room temperature. For TPR investigation, the temperature range was 100–900 °C and the heating rate was 15 °C min^{-1}.

The adsorption of a particular gas was carried out at 170 °C using apparatus and following procedure similar to that described by Chafik et al. [38]. In a typical experiment, 300 mg of the catalyst was placed in a quartz microreactor and heated to 500 °C and kept at this temperature in flowing Ar for 1 h before being cooled to 170 °C in Ar. The reactor was then exposed to a flow of desired gas for adsorption. After the adsorption process, the sample was purged with Ar for 40 min before TPD recording (linear ramping to 600 °C, rate = 10 °C min^{-1}).

Analysis of gases in effluent was done by employing an on-line mass spectrometer (MS, Omini-star, GSD-300) equipped with a fast-response inlet capillary/leak diaphragm system and an infrared absorption spectrometer (IRAS, SICK-MAIHAK, S710). Since CO and N_2 are of m/z = 28 while CO_2 and N_2O are

of $m/z = 44$, the two pairs of gaseous molecules cannot be analyzed by MS alone. Instead, the presence of CO, N_2O and CO_2 in the gas-phase was determined by IRAS. The composition of the gas used in the adsorption process was CO (800 ppm) and NO (800 ppm), respectively, and the flow rate was 75 $cm^3\ min^{-1}$. The flow rate of carrier gas for MS measurement was 50 $cm^3\ min^{-1}$. The MS signals at $m/z = 18$ (H_2O^+), 28 (CO^+ and N_2^+), 30 (NO^+), 32 (O_2^+), 40 (Ar^+), and 44 (CO_2^+ and N_2O^+) were recorded continuously. When necessary (e.g. for the analysis of signal intensities of CO_2 and CO), the cracking coefficient determined in separate experiments was taken into account.

3. Results

3.1. Catalytic activities

3.1.1. Effect of supports

The conversion of NO and CO as related to reaction temperature over NiO/γ-Al_2O_3, NiO/TiO_2, and NiO/CeO_2(DP) in the NO/CO test are shown in Fig. 1. The results demonstrated that NiO/CeO_2(DP) is superior to NiO/γ-Al_2O_3 and NiO/TiO_2 in catalytic activity. The NiO/CeO_2(DP) catalyst was active from 100 °C onwards, and showed 100% NO and CO conversions at 250 °C. Over NiO/γ-Al_2O_3, one had to raise the temperature to 550 °C to reach NO and CO conversion of ca. 98%. Over NiO/TiO_2, NO and CO conversion were below 85% even at a temperature as high as 600 °C. One can see that catalytic activity below 250 °C over NiO/γ-Al_2O_3 and NiO/TiO_2 was insignificant, and the first few data points (with conversion below 5%) could be due to NO and CO adsorption rather than NO and CO conversion.

3.1.2. Effect of CeO_2 prepared with different methods

The NO and CO conversion over the CeO_2(DP), CeO_2(PC), CeO_2(HP), NiO/CeO_2(DP), NiO/CeO_2(PC), NiO/CeO_2(HP), and NiO samples are shown in Table 1. The three ceria samples showed catalytic activity for the NO/CO reaction. Among them, the ceria prepared by the HP method displayed NO and CO conversion slightly higher than those of the ceria prepared by the DP and PC method. With loading of NiO on the ceria samples, there was significant enhancement in performance. The NiO/CeO_2(HP) catalyst showed significant activity from 100 °C onwards for CO oxidation to CO_2 and from 150 °C onwards for NO reduction to N_2, and there was complete NO and CO conversion at 210 °C, a temperature ca. 20 °C lower than that for complete NO and CO conversion over NiO/CeO_2(DP) and NiO/CeO_2(PC). It is clear that the method of CeO_2 preparation is crucial to the catalytic nature of ceria. The activity of NiO/CeO_2(DP), NiO/CeO_2(PC), and NiO/CeO_2(HP)

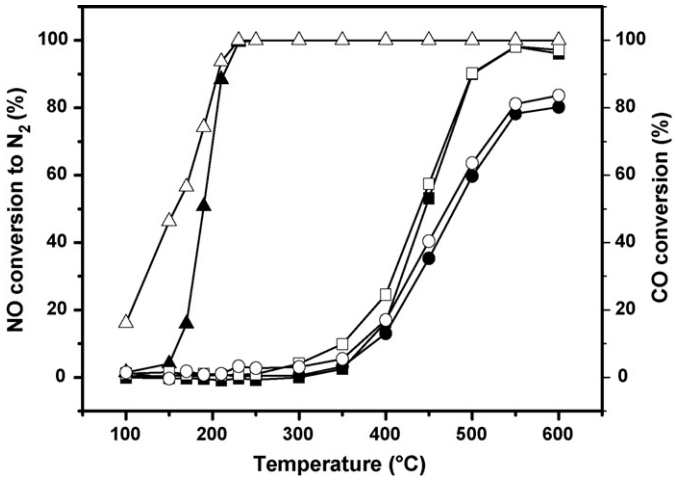

Fig. 1. NO (solid symbols) and CO (hollow symbols) conversion vs. reaction temperature over NiO/γ-Al_2O_3 (square), NiO/TiO_2 (circle), and NiO/CeO_2(DP) (triangle) for the investigation of effect of support on catalytic performance of NiO in NO–CO reaction. Gas composition: 2500 ppm NO, 2500 ppm CO and the balance of He; and reaction conditions: catalyst weight = 0.1 g; total flow rate = 75 $cm^3\ min^{-1}$; GHSV = 120,000 h^{-1}.

Table 1
Activity of CeO_2 and NiO/CeO_2 samples for NO reduction with CO

Conversion (%)														
Catalyst T (°C)	CeO_2(DP)		NiO/CeO_2(DP)		CeO_2(PC)		NiO/CeO_2(PC)		CeO_2(HP)		NiO/CeO_2(HP)		NiO	
	NO	CO	NO	CO	NO	CO	NO	CO	NO	CO	NO	CO	NO	CO
100	0	0	2	16	0	0	1	16	0	0	1	22	0	0
150	0	0	4	46	0	0	3	42	0	0	13	56	0	2
170	0	0	16	56	0	0	10	53	0	0	50	74	0	2
190	0	0	51	74	0	0	41	71	0	0	90	94	0	0
210	0	0	88	94	0	0	77	89	0	0	100	100	0	0
230	1	2	99	100	0	0	96	98	3	3	100	100	0	2
250	2	3	100	100	1	2	100	100	4	5	100	100	0	4
300	10	11	100	100	7	7	100	100	13	11	100	100	8	9
350	29	30	100	100	23	21	100	100	36	36	100	100	29	33
400	55	54	100	100	47	48	100	100	63	61	100	100	53	58
450	77	76	100	100	72	72	100	100	88	83	100	100	78	84
500	96	95	100	100	92	93	100	100	100	97	100	100	84	90
550	100	100	100	100	100	100	100	100	100	100	100	100	99	100
600	100	100	100	100	100	100	100	100	100	100	100	100	100	100

Reaction conditions: catalyst weight = 0.1 g; total flow rate = 75 $cm^3\ min^{-1}$; GHSV = 120,000 h^{-1}.

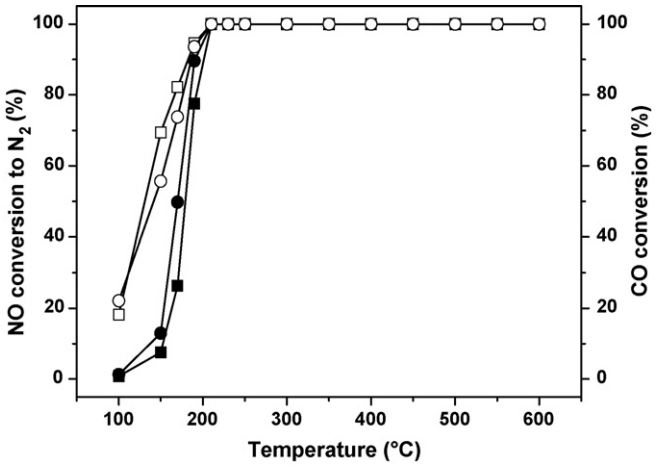

Fig. 2. NO (solid symbols) and CO (hollow symbols) conversion vs. reaction temperature over NiO/CeO_2(HP) for the investigation of effect of oxygen in the feed on catalytic activity (square symbols: NO–CO; circle symbols: NO–CO–O_2). NO–CO feed: 2500 ppm NO, 2500 ppm CO and balance of He; NO–CO–O_2 feed: 2500 ppm NO, 5000 ppm CO, 1250 ppm O_2 and balance of He. Reaction conditions are the same as those of Fig. 1.

was far better than that of CeO_2(DP), CeO_2(PC), CeO_2(HP), and NiO. Despite the NiO/CeO_2(DP), NiO/CeO_2(PC), and NiO/CeO_2(HP) catalysts could be considered as ''Ce-rich'', the temperature for complete NO and CO conversion over them was far lower than that over CeO_2, indicating that the introduction of a small amount of nickel in CeO_2 can promote significantly the catalytic activity of CeO_2.

3.1.3. Effect of O_2

The results of catalytic activity over NiO/CeO_2(HP) for the NO/CO and NO/CO/O_2 reaction are shown in Fig. 2. One can detect that CO oxidation with NO (responsible for CO conversion at temperature $\leq$210 °C) was only slightly affected by the presence of O_2 in the reactant feed, but NO reduction with CO (responsible for NO conversion to N_2 at temperature $\leq$210 °C) was obviously affected by O_2 presence. The result is in contrast to the behavior observed over noble metal catalysts promoted by ceria-related oxides. Under conditions similar to those employed here, the activity of NO reduction with CO decreased when there was O_2 in the feed [47].

3.2. Characterization of NiO/CeO_2(HP)

3.2.1. XRD

Fig. 3 shows the XRD pattern of the CeO_2(HP) support as well as that of NiO and NiO/CeO_2(HP) catalyst. By making reference to the patterns of CeO_2(HP) and NiO, one can only detect very weak signals of NiO crystallites in the XRD pattern of NiO/CeO_2(HP). In other words, there was good dispersion of NiO in the NiO/CeO_2(HP) catalyst.

3.2.2. H_2-TPR

Fig. 4A shows the TPR profiles of the CeO_2(HP), CeO_2(DP) and CeO_2(PC) samples. There are two reduction peaks in each profile, one at ca. 505–534 °C, and the other at ca. 787–817 °C, corresponding to the reduction of surface and bulk oxygen

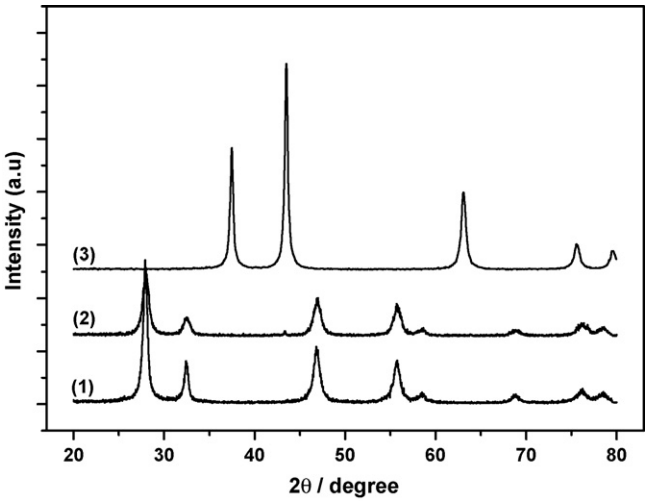

Fig. 3. XRD patterns of (1) CeO_2(HP), (2) NiO/CeO_2(HP), and (3) NiO.

species [48–50]. It is believed that during the reduction, there is a decrease in oxidation state of the cerium ions. With the presence of NiO, there are significant changes in the features of TPR profiles (Fig. 4B). There are three hydrogen consumption peaks (labeled α, β and γ) detected over the NiO/CeO_2 catalysts. The γ peak at ca. 818 °C is ascribed to the reduction

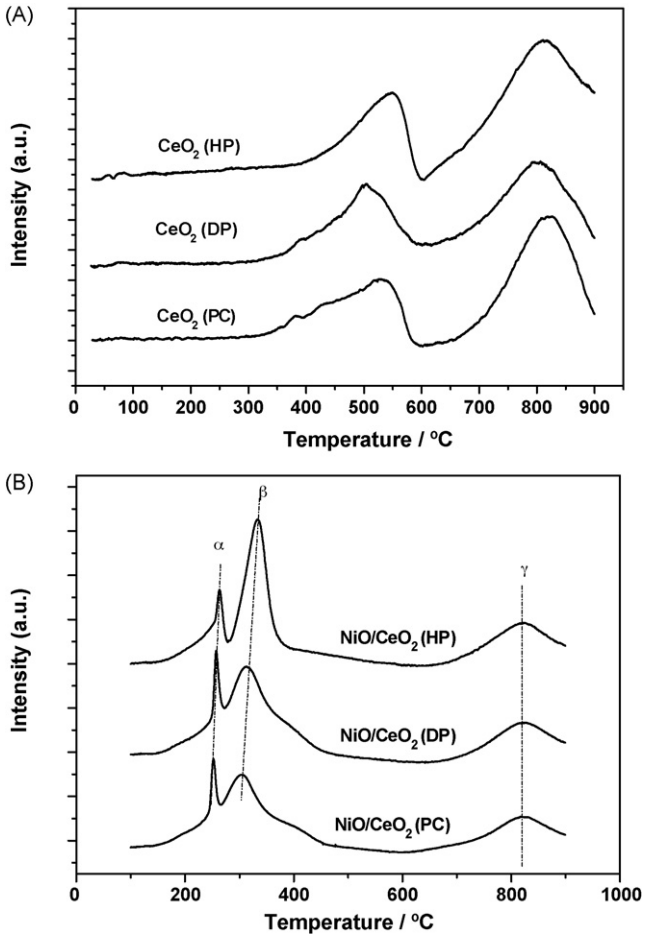

Fig. 4. H_2-TPR spectra of CeO_2 (A) and NiO/CeO_2 (B) samples pre-treated in He stream at 500 °C for 1 h.

of crystalline CeO_2. The β peak at ca. 320 °C (only slightly lower in temperature than the reduction peak of a standard NiO sample) is due to the reduction of NiO (to Ni^0) that is strongly bound to the CeO_2 support [51]. The α peak at ca. 263 °C can be ascribed to the reduction of free NiO particles [52]. It is interesting to observe that among the three catalysts, NiO/CeO_2(HP) shows the highest temperature and intensity for β reduction. There is a gradual shift of α and β peaks to lower temperatures over the NiO/CeO_2(DP) and NiO/CeO_2(PC) catalysts. The phenomena implied that the interaction between NiO and CeO_2 is the highest inside the NiO/CeO_2(HP) catalyst.

3.3. Mechanism studies

3.3.1. CO- and NO-TPD

The adsorption of CO on a NiO/CeO_2(HP) sample pre-treated at 500 °C in Ar was conducted at room temperature. The CO-TPD profiles are shown in Fig. 5. The CO_2 desorption profile ranging from ca. 150 to 550 °C shows a rather symmetric peak at 350 °C and a shoulder at ca. 250 °C. The 350 °C peak can be related to CO interaction with the NiO that binds strongly to CeO_2 and the shoulder peak to CO interaction with free NiO particles [51]. There are two CO desorption peaks, one at 85 °C and one at 350 °C with the former bigger than the latter. The former is due to weakly bound CO, and the latter should be ascribed to the MS fragment of CO_2.

The NO-TPD profiles after NO adsorption at 170 °C on a NiO/CeO_2(HP) sample (pre-treated at 500 °C in Ar) are shown in Fig. 6. With a rise in sample temperature, there is desorption of NO and O_2. The profile of NO desorption shows peaks at 260 and 410 °C with the latter coinciding the major desorption peak of O_2. The former is originated from the strongly adsorbed NO species. It is obvious that the latter is due to the decomposition of adsorbed NO_x ($x = 2$ or 3) species (giving peaks of NO and O_2) at elevated temperatures [53]. There is no desorption of N_2O and N_2

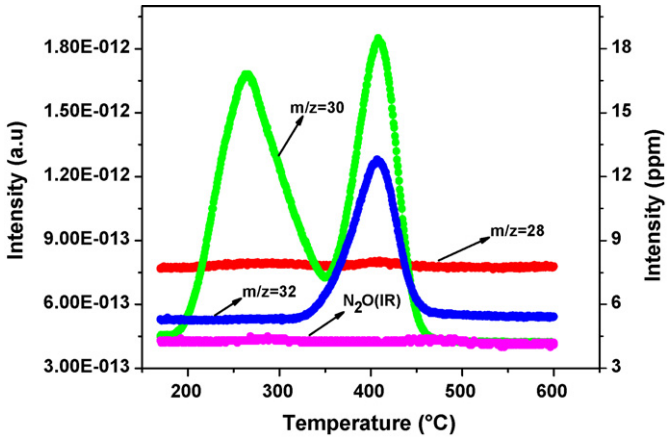

Fig. 6. NO-TPD results obtained following NO adsorption at 170 °C on NiO/CeO_2(HP).

3.3.2. NO adsorption on NiO/CeO_2 and NO displacement by CO

A NiO/CeO_2(HP) sample pre-treated at 500 °C in Ar was exposed to a flow of 0.08% NO/He at 170 °C until there was no more NO adsorption as reflected in the restoration of the NO signal to that of the NO feed. As shown in Fig. 7, after an on-stream time of 1 min, there is the detection of NO and N_2O, the signal of the latter comes to a maximum at 2.3 min on-stream and declines as the signal of NO increases to its full capacity in a period of ca. 30 min.

Following this treatment, the sample was purged with Ar for 40 min and then exposed to a flow of 0.08%CO/He. From Fig. 8, it is observed that there is detection of CO_2 and NO after an on-stream time of ca. 2 min. At 10 min, the signals of CO_2 and NO decrease while that of CO appears. After about 35 min, the signal of CO reaches its full capacity, indicating the end of CO adsorption. The results of the subsequent TPD experiment are shown in Fig. 9. Since the effluent shows no IR signal of N_2O, the $m/z = 44$ mass signal should be ascribed to CO_2. It is observed that the CO_2 profile exhibits an intense and broad peak at 320 °C with a shoulder at 210 °C. Despite lower in intensity,

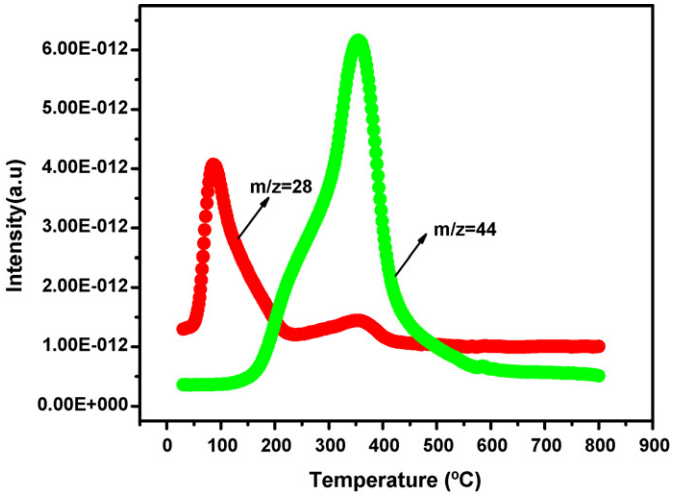

Fig. 5. CO-TPD results obtained following CO adsorption at RT on NiO/CeO_2(HP).

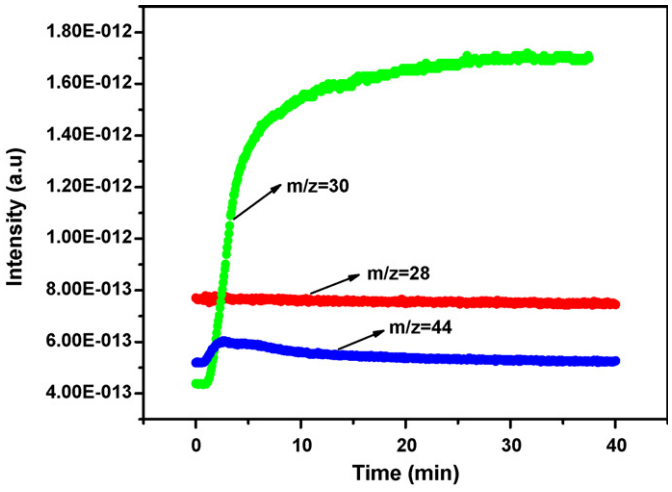

Fig. 7. MS signals (at $m/z = 28$, 30 and 44) obtained when NiO/CeO_2(HP) was exposed to a flow of 0.08% NO/Ar at 170 °C.

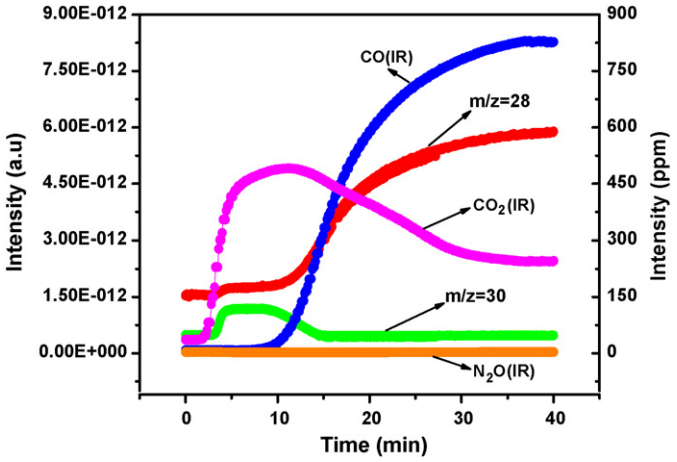

Fig. 8. IR responses of gas-phase CO, CO_2, and N_2O, and MS signals at $m/z = 28$ and 30 obtained when the NiO/CeO_2(HP) sample of Fig. 7 (after exposure to 0.08% NO/Ar flow at 170 °C for 40 min and purging with Ar for 40 min) was exposed to a flow of 0.08%CO/Ar at 170 °C.

the $m/z = 28$ signal shows a profile similar to that of $m/z = 44$, indicating that the $m/z = 28$ signal is part of the cracking pattern of CO_2. In other words, there is no detection of N_2.

3.3.3. CO adsorption on NiO/CeO_2 and CO displacement by NO

A NiO/CeO_2(HP) sample pre-treated at 500 °C in Ar was exposed to a flow of 0.08%CO/He at 170 °C (Fig. 10). The interaction of CO with the catalyst results in the formation of CO_2 which comes to a maximum at 20 min after the introduction of CO, and then declines gradually with time-on-stream. At about 30 min, the CO signal intensity returns to that of the feed, indicating the cease of CO interaction with the catalyst. The system was then purged with Ar for 40 min and a flow of 0.08% NO/Ar was introduced to the reactor at 170 °C. It is observed from Fig. 11 that during the first 1 min after exposure to 0.08% NO/Ar, only N_2 appears at the exit of the reactor. At ca. 3 min, there is the detection of CO_2 in the effluent. Then at ca. 20 min, NO begins to evolve and the yield

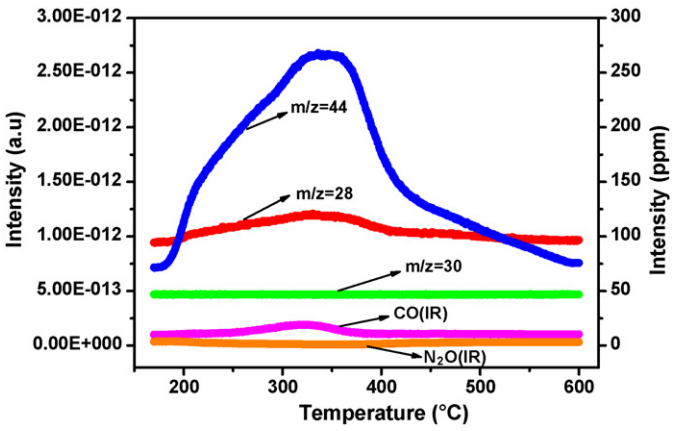

Fig. 9. IR responses of gas-phase CO and N_2O, and MS signals at $m/z = 28$, 30 and 44 obtained when the NiO/CeO_2(HP) sample of Fig. 8 (after exposure to 0.08%CO/Ar flow) was subject to TPD investigation in Ar stream.

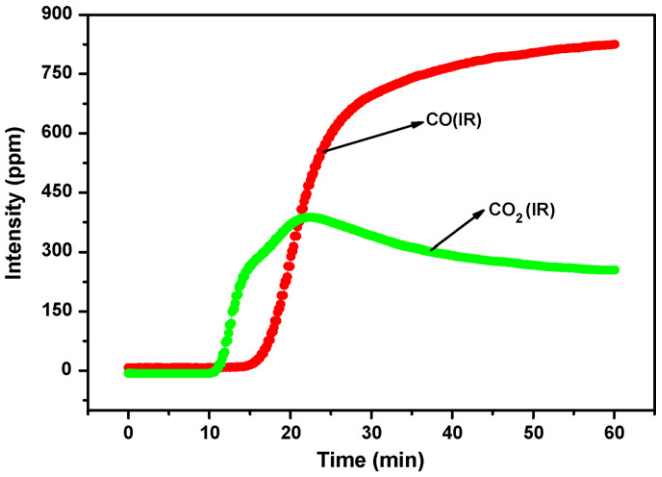

Fig. 10. IR responses of gas-phase CO and CO_2 obtained when a NiO/CeO_2(HP) sample was exposed to a flow of 0.08%CO/Ar at 170 °C.

of N_2 and CO_2 start to decline. Accompanied by the appearance of NO is the formation of N_2O, and the N_2O yield comes to a maximum at 26 min and then drops. After 30 min, the signal intensity of NO reaches that of the feed, indicating the cease of all adsorption and/or reaction processes. The results of the subsequent TPD experiments are shown in Fig. 12. The NO profile displays two maxima, an intense one at 250 °C and a minor one at 420 °C. As indicated in Fig. 6 of the NO-TPD experiment, the peak at 250 °C can be ascribed to the strongly adsorbed NO, while the one at higher temperature to the NO generated in the decomposition of NO_x ($x = 2$ or 3) [53]. Accompanying the NO desorptions are those of O_2, N_2, N_2O, and CO_2. The profile of O_2 shows a peak at 420 °C whereas that of N_2, N_2O, and CO_2 exhibit a maximum at 260 °C.

3.3.4. NO adsorption on CO-prereduced NiO/CeO_2

The catalyst was first treated in 0.08%CO/Ar at 170 °C for 1 h, and then flushed with Ar at 600 °C for 1 h to remove adsorbed CO. The catalyst was then cooled to 170 °C and exposed to a feed of 0.08% NO/Ar until there was no further

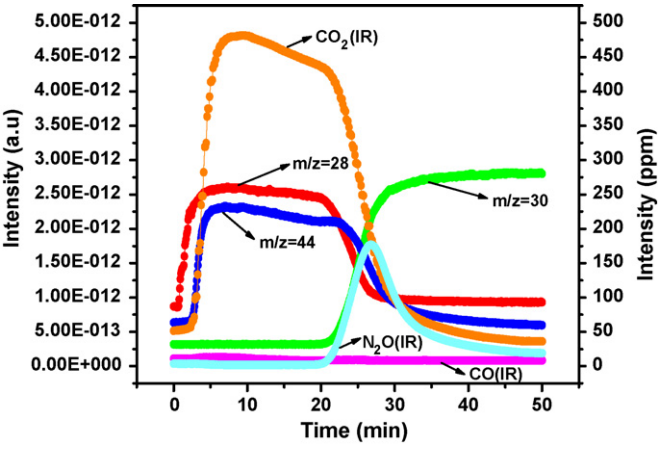

Fig. 11. IR responses of gas-phase CO, CO_2, and N_2O, and MS signals at $m/z = 28$, 30 and 44 obtained when the NiO/CeO_2(HP) sample of Fig. 10 (after exposure to 0.08%CO/Ar flow at 170 °C for 40 min and purging with Ar for 40 min) was exposed to a flow of 0.08% NO/Ar at 170 °C.

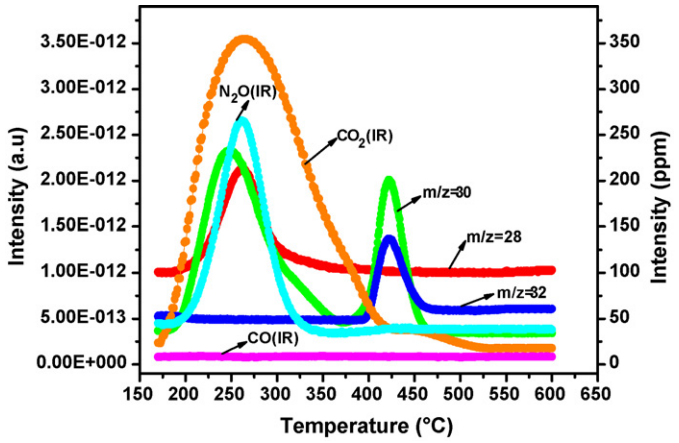

Fig. 12. IR responses of gas-phase CO, CO_2, and N_2O, and MS signals at $m/z = 28$, 30 and 32 obtained when the NiO/CeO_2(HP) sample of Fig. 11 (after exposure to 0.08% NO/Ar flow) was subject to TPD investigation in Ar stream.

NO adsorption. From Fig. 13, one can see that the N_2 signal appears immediately after the sample was exposed to 0.08% NO/Ar, and the N_2 signal comes to a maximum after ca. 4 min on-stream. There is a shoulder peak at ca. 2.5 min and the yield of N_2 decreases abruptly when NO starts to evolve. The evolution of NO is accompanied by the formation of N_2O, and the yield of N_2O peaks at 10 min and then decreases. After 20 min, the signal of NO reaches that of the 0.08% NO/Ar feed, indicating the cease of NO adsorption and reaction processes.

4. Discussion

4.1. Effects of nickel–ceria interaction

A close nickel–ceria contact is thought to be crucial and is related to the high activities exhibited in the reduction of NO by CO. As evidenced by the H_2-TPR results of Fig. 4, the obvious shift toward higher temperature and the detection of stronger β reduction peak suggest strong interaction between nickel and

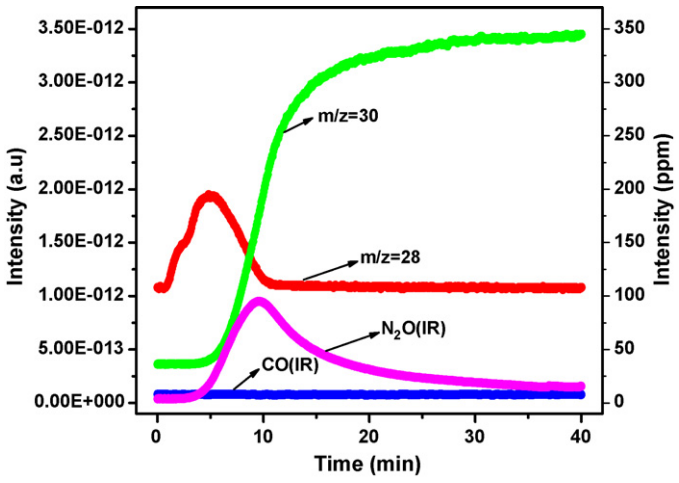

Fig. 13. IR responses of gas-phase CO and N_2O, and MS signals at $m/z = 28$ and 30 obtained when a NiO/CeO_2(HP) sample pre-reduced by CO at 170 °C (in 0.08%CO/Ar flow at 170 °C for 1 h and then flushed with Ar at 600 °C) was exposed to a flow of 0.08% NO/Ar at 170 °C for 1 h.

ceria in NiO/CeO_2(HP). By impregnating nickel nitrate into ceria powder, it is possible that certain amounts of Ni^{2+} ions have incorporated into the ceria lattice. For example, Shan et al. reported the formation of a $Ce_{1-x}Ni_xO_2$ solid solution as evidenced by the variation of ceria lattice parameters induced by the addition of Ni [46]. Because the radius of Ni^{2+} (0.072 nm) is smaller than that of Ce^{4+} (0.101 nm), and the oxidation state of Ni^{2+} is different from that of Ce^{4+}, charge unbalance and lattice distortion occur within the structure of CeO_2 when there is partial replacement of Ce^{4+} by Ni^{2+}. Generally speaking, the formation of $Ce_{1-x}Ni_xO_2$ via the incorporation of Ni^{2+} ions into ceria lattice leads to the generation of oxygen vacancies on which oxygen adsorption is facile [51,52]. The oxygen species thus adsorbed are very active for NO/CO reaction.

4.2. Reaction mechanism

In previous works, it was demonstrated that the mechanism involving NO dissociation is only applicable to zero-valent metal catalysts, and the model is not appropriate to explain the catalysis of non-noble metal oxides [54–57]. In our investigation, we obtained results which indicated the involvement of dissociative adsorption of nitric oxide in the process of NO reduction by CO over the NiO/CeO_2(HP) catalyst.

4.2.1. Interaction of NO with calcined NiO/CeO_2 and NO displacement by CO

With the exposure of calcined NiO/CeO_2(HP) to NO(0.08%)/Ar at 170 °C, there is the appearance of N_2O after around 1 min of interaction (Fig. 7). According to Martinez-Arias et al. [58], there is the formation of hyponitrite when two NO molecules are located closely at a "Ce^{3+}-oxygen vacancy" site and the decomposition of hyponitrites would result in the evolution of N_2O. Reactions (1) and (2) account for the formation of N_2O (* denotes a vacant site):

$$2NO + * \leftrightarrow NO * NO \quad (1)$$

$$NO * NO \leftrightarrow N_2O + *O \quad (2)$$

with the occupancy of active sites by surface oxygen atoms, there is the gradual decline in N_2O generation. After around 25 min, NO is detected in the effluent and NO adsorption comes to a final stop. Combining the phenomena with those observed in the NO-TPD experiments (Fig. 6), one can see that there are two kinds of NO adsorption on the catalyst: one is in the form of *NO, and the other is in the form of $*NO_x$ ($x = 2$ or 3):

$$NO + * \leftrightarrow *NO \quad (3)$$

$$NO + x*O \leftrightarrow *NO_x \quad (4)$$

since there is no N_2 production during the NO adsorption process, one can deduce that NO adsorption on calcined NiO/CeO_2 was associative. The results of MS investigation for the probing of CO interaction with surface NO at 170 °C show that exposure of such a surface to CO leads to a rapid formation of CO_2 accompanied by the emission of NO (Fig. 8).

The appearance of CO_2 immediately after CO introduction evidenced that the catalyst has been partially oxidized during exposure to NO:

$$CO + *O \leftrightarrow CO_2 + * \quad (5)$$

$$CO + *NO \leftrightarrow NO + *CO \quad (6)$$

$$CO + *NO_x + * \leftrightarrow NO + *CO + x*O \quad (7)$$

with time-on-stream, the catalyst surface is depleted of *O, *NO and *NO_x, and the generation of CO_2 drops gradually. The CO_2 profile shows a long tail, indicating that the incoming CO also interacts with the oxygen atoms of ceria:

$$CeO_2 + xCO \rightarrow CeO_{2-x} + xCO_2 \quad (8)$$

apart from CO_2 and NO, no N_2 is produced during the adsorption process. Results of the TPD process that followed showed that with a rise in temperature, the adsorbed CO reacted with surface oxygen to produce CO_2, while there was a small amount of CO desorption at about 330 °C. It is worth noting that the curve of $m/z = 28$ should be related to the cracking of CO_2 ($m/z = 44$) and CO desorption, rather than the forming of N_2.

Based on the points discussed so far, it is clear that during the NO adsorption process, NO does not dissociate to produce nitrogen atoms over an oxidized surface of NiO/CeO_2(HP). When CO interacts with the adsorbed NO, there is no detection of N_2 in the effluent, suggesting that both the *NO and *NO_x species do not react directly with CO to produce N_2. In other words, it is not feasible to have NO reduced by CO via such a route.

4.2.2. Interaction of CO with calcined NiO/CeO_2 and CO displacement by NO

As shown in Figs. 10 and 11, exposure of a calcined NiO/CeO_2(HP) catalyst to CO leads to CO_2 generation and the regeneration of active sites (*):

$$CO + * \rightarrow *CO \quad (9)$$

$$*CO + *O \rightarrow CO_2 + 2* \quad (10)$$

with the depletion of surface *O, there is a decline in CO_2 generation. Due to the consumption of surface *O, there is a decrease in CO_2 formation rate. When surface *O is depleted, the generation of CO_2 ceases. Interaction of NO with a NiO/CeO_2(HP) sample pre-exposed to CO results in the evolution of N_2 and CO_2. As shown in Fig. 13, there is immediate detection of N_2 when the reduced sample was exposed to NO. The surface oxygen atoms generated in NO dissociation at reduced sites react with surface CO to produce CO_2. In addition, there is no detection of CO desorption, implying that there is no displacement of adsorbed CO species by the incoming NO molecules. After an on-stream time of around 20 min, because of the consumption of surface N atoms and the accumulation of adsorbed NO species, the reaction between *NO and *N becomes significant, resulting in maximum formation of N_2O at 26 min. With the depletion of surface *N, the reaction ceases, and the signal intensity of NO reaches that of the feed.

The phenomena described above can be related to the following reaction steps:

$$NO + * \leftrightarrow *NO \quad (11)$$

$$*NO + * \rightarrow *N + *O \quad (12)$$

$$*N + *N \rightarrow N_2 + 2* \quad (13)$$

$$*CO + *O \rightarrow CO_2 + 2* \quad (14)$$

$$*NO + *N \rightarrow N_2O + 2* \quad (15)$$

A rise in sample temperature during TPD investigation would result in steps (3) and (4) shifting to the left, i.e. desorption of *NO and decomposition of *NO_x. As adsorbed CO reacts with surface O to yield CO_2, new reduced sites are generated on the catalyst to enable the dissociation of NO to yield N_2 and N_2O.

It is apparent that during the CO adsorption process, there is the reduction of catalyst and the formation of *CO. Considering that the possibility of having *CO reacting directly with NO on a pre-reduced catalyst would cause ambiguity in the reasoning of nitrogen production, we removed adsorbed CO first by means of high-temperature treatment and then had NO introduced to the treated surface which should be free of adsorbed CO. Combining the so-obtained results with those of Fig. 13, it is clear that CO reduction of surface oxygen for the generation of vacancies is the first and critical step, and the dissociation of NO on the reduced surface is the pathway for N_2 generation.

5. Conclusion

The ceria-supported NiO catalysts exhibited activity for stoichiometric NO/CO reaction much higher than that detected over the NiO supported on γ-Al_2O_3 and TiO_2(P25). The interfacial synergism of nickel and ceria as evidenced by the generation of easily reduced oxygen species has been proposed to be the reason for the higher catalytic activities, and the redox action at the interface is considered to be crucial for good catalytic activity. A model for NO + CO interaction over NiO/CeO_2 involves the following steps: (i) reduction of catalyst surface by CO and the generation of vacant sites; (ii) dissociative adsorption of NO at vacant sites; and (iii) scavenging surface O by CO. With the regeneration of surface vacant sites, inhibiting effect of oxygen accumulation is avoided.

Acknowledgements

This work was supported by National Natural Science Foundation of China (No. 20573014) and Program for New Century Excellent Talents in University (NCET-07-0136).

References

[1] M. Shelef, G.W. Graham, Catal. Rev. Sci. Eng. 36 (1994) 433.
[2] J.N. Armor, Appl. Catal. B: Environ. 1 (1992) 221.
[3] K.C. Taylor, Catal. Rev. Sci. Eng. 35 (1993) 457.
[4] A.B. Hungria, J.J. Calrino, J.A. Anderson, A. Martinez-Arias, Appl. Catal. B: Environ. 62 (2006) 359.

[5] A.B. Hungria, N.D. Browning, R.P. Erni, M. Fernandez-Garcia, J.C. Conesa, J.A. Perez-Omil, A. Martinez-Arias, J. Catal. 235 (2005) 251.
[6] S. Xu, X. Yan, X. Wang, Fuel 85 (2006) 2243.
[7] M. Fernandez-Garcia, E. Comez Rebollo, A. Guerrero Ruiz, J.C. Conesa, J. Soria, J. Catal. 172 (1997) 146.
[8] M. Boaro, F. Giordano, S. Recchia, V.D. Santo, M. Giona, A. Trovarelli, Appl. Catal. B: Environ. 521 (2004) 225.
[9] H.X. Mai, L.D. Sun, Y.W. Zhang, R. Si, W. Feng, H.P. Zhang, H.C. Liu, C.H. Yan, J. Phys. Chem. B 109 (2005) 24380.
[10] A. Martinez-Arias, R. Cataluna, J.C. Conesa, J. Soria, J. Phys. Chem. B 102 (1998) 809.
[11] A. Martinez-Arias, M. Fernandez-Garcia, A.B. Hargria, A. Iglesias-Juez, K. Duncan, R. Smith, J.A. Anderson, J.C. Conesa, J. Soria, J. Catal. 204 (2001) 238.
[12] L. Ilieva, G. Pantaleo, I. Ivanov, A.M. Venezia, D. Andreeva, Appl. Catal. B: Environ. 65 (2006) 101.
[13] W. Ruettinger, X.S. Liu, R.J. Farrauto, Appl. Catal. B: Environ. 65 (2006) 135.
[14] X. Wang, J.A. Rodriguez, J.C. Hanson, D. Gamarra, A. Martinez-Arias, M. Fernandez-Garcia, J. Phys. Chem. B 110 (2006) 428.
[15] Y. Li, Q. Fu, M. Flytzani-Stephanopoulos, Appl. Catal. B: Environ. 27 (2000) 179.
[16] J.B. Wang, D. Tsai, T. Huang, J. Catal. 208 (2002) 370.
[17] M. Lou, X. Yuan, X. Zheng, Appl. Catal. A: Gen. 175 (1998) 121.
[18] P. Bera, S.T. Aruna, K.C. Patil, M.S. Hegde, J. Catal. 186 (1999) 36.
[19] G. Ranga Rao, P. Fornasiero, R. Di Monte, J. Kaspar, G. Vlaic, G. Balducci, S. Meriani, G. Gubitosa, A. Cremona, M. Graziani, J. Catal. 162 (1996) 1.
[20] X. Jiang, L. Lou, Y. Chen, X. Zheng, J. Mol. Catal. A: Chem. 197 (2003) 193.
[21] D. Ciuparu, A. Bensalem, L. Pfefferle, Appl. Catal. B: Environ. 26 (2000) 241.
[22] T. Ohno, F. Hatayama, Y. Toda, S. Konishi, H. Miyata, Appl. Catal. B: Environ. 5 (1994) 89.
[23] T. Ohno, Y. Bunno, F. Hatayama, Y. Toda, H. Miyata, Appl. Catal. B: Environ. 30 (2001) 421.
[24] Y.H. Hu, L. Dong, M.M. Shen, D. Liu, J. Wang, W.P. Ding, Y. Chen, Appl. Catal. B: Environ. 31 (2001) 61.
[25] L. Ma, M.F. Luo, S.Y. Chen, Appl. Catal. A: Gen. 242 (2003) 151.
[26] X.Y. Jiang, L.P. Lou, Y.X. Chen, X.M. Zheng, J. Mol. Catal. A: Chem. 197 (2003) 193.
[27] A. Martínez-Arias, M. Fernández-García, J. Soria, J.C. Conesa, J. Catal. 214 (2003) 261.
[28] E.F. Iliopoulou, E.A. Efthimiadis, I.A. Vasalos, Ind. Eng. Chem. Res. 43 (2004) 1388.
[29] E.F. Iliopoulou, A.P. Evdou, A.A. Lemonidou, I.A. Vasalos, Appl. Catal. A: Gen. 274 (2004) 179.
[30] N.A.S. Amin, E.F. Tan, Z.A. Manan, Appl. Catal. B: Environ. 20 (2003) 57.
[31] M. Fernández-García, A. Martínez-Arias, A. Iglesias-Juez, A.B. Hungría, J.A. Anderson, J.C. Conesa, J. Soria, J. Catal. 214 (2003) 220.
[32] C.Y. Lee, T.H. Jung, B.H. Ha, Appl. Catal. B: Environ. 9 (1996) 77.
[33] L.F. Liotta, G. Pantaleo, G. Di Carlo, G. Marci, G. Deganello, Appl. Catal. B: Environ. 52 (2004) 1.
[34] V.I. Parvulescu, P. Grange, B. Delmon, Catal. Today 46 (1998) 233.
[35] P. Granger, L. Delannoy, J.J. Lecomte, C. Dathy, H. Praliaud, L. Leclercq, G. Leclercq, J. Catal. 235 (2005) 251.
[36] D. Chatterjee, O. Deutschmann, J. Warnatz, Faraday Discuss. 119 (2001) 371.
[37] S. Roy, A. Marimuthu, M.S. Hegde, G. Madras, Appl. Catal. B: Environ. 71 (2007) 23.
[38] T. Chafik, D.I. Kondarides, X.E. Verykios, J. Catal. 190 (2000) 446.
[39] F. Fajardie, J.F. Tempere, J.M. Manoli, O. Touret, G. Blanchard, G.D. Mariadassou, J. Catal. 179 (1998) 469.
[40] S.S.C. Chuang, C.-D. Tan, J. Catal. 173 (1998) 95.
[41] G. Vlaic, R.D. Monte, P. Fornasiero, E. Fonda, J. Kaspor, M. Graziani, J. Catal. 182 (1999) 378.
[42] J.W. London, A.T. Bell, J. Catal. 31 (1973) 96.
[43] R.T. Rewick, H. Wise, J. Catal. 40 (1975) 301.
[44] C. Lamonier, A. Ponchel, A. D'Huysser, L. Jalowiecki-Duhamel, Catal. Today 50 (1999) 247.
[45] A. Saadi, R. Merabti, Z. Rassoul, M.M. Bettahar, J. Mol. Catal. A: Chem. 253 (2006) 79.
[46] W.J. Shan, M.F. Luo, P.L. Ying, W.J. Shen, C. Li, Appl. Catal. A: Gen. 246 (2003) 1.
[47] D.I. Kondarides, T. Chafik, X.E. Verykios, J. Catal. 191 (2000) 147.
[48] F. Giordano, A. Trovarelli, C. de Leitenburg, M. Giona, J. Catal. 193 (2000) 273.
[49] S. Damyanova, C.A. Perez, M. Schmal, J.M.C. Bueno, Appl. Catal. A: Gen. 234 (2002) 271.
[50] H.Y. Zhang, A.M. Zhu, X.K. Wang, Y. Wang, C. Shi, Catal. Commun. 8 (2007) 612.
[51] K.V.R. Chary, P.V.R. Rao, V. Vishwanathan, Catal. Commun. 7 (2006) 974.
[52] Y. Li, B.C. Zhang, X.L. Tang, Y.D. Xu, W.J. Shen, Catal. Commun. 7 (2006) 380.
[53] C. Shi, M. Cheng, Z. Qu, X. Bao, Appl. Catal. B: Environ. 51 (2004) 171.
[54] A.R. Balkenende, C.J.G. Vander Gift, E.A. Meulenkamp, J.W. Geus, Appl. Surf. Sci. 68 (1993) 161.
[55] A.T.S. Wee, J. Lin, A.C.H. Huan, F.C. Loh, K.L. Tan, Surf. Sci. 304 (1994) 145.
[56] F. Boccuzzi, M. Baricco, E. Guglielminotti, Appl. Surf. Sci. 70–71 (1993) 147.
[57] F. Boccuzzi, E. Guglielminotti, G. Martra, G. Gerrato, J. Catal. 146 (1994) 449.
[58] A. Martinez-Arias, J. Soria, J.C. Conesa, X.L. Seoane, A. Arcoya, R. Cataluna, J. Chem. Soc., Faraday Trans. 91 (1995) 1679.